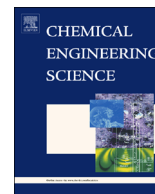




Contents lists available at ScienceDirect

## Chemical Engineering Science

journal homepage: [www.elsevier.com/locate/ces](http://www.elsevier.com/locate/ces)

# Microneedle assisted micro-particle delivery by gene guns: Mathematical model formulation and experimental verification

Dongwei Zhang, Diganta B. Das\*, Chris D. Rielly

Department of Chemical Engineering, Loughborough University, Loughborough, LE11 3TU, Leicestershire, UK

## HIGHLIGHTS

- Microneedle (MN) assisted micro-particle delivery enhances particle penetration.
- Mathematical model for MN assisted micro-particles delivery is developed.
- Results are validated with experimental results obtained from the previous work.
- Developed model is used to simulate velocity and trajectories of micro-particles.
- MNs assist in reducing operating pressures for gene guns.

## ARTICLE INFO

## Article history:

Received 14 December 2013

Received in revised form

13 June 2014

Accepted 18 June 2014

## Keywords:

Modelling

Gene gun

Micro-particle

Microneedle

Penetration depth

## ABSTRACT

Gene gun is a micro-particles delivery system which accelerates DNA loaded micro-particles to a high speed so as to enable penetration of the micro-particles into deeper tissues to achieve gene transfection. Previously, microneedle (MN) assisted micro-particles delivery has been shown to achieve the purpose of enhanced penetration depth of micro-particles based on a set of laboratory experiments. In order to further understand the penetration process of micro-particles, a mathematical model for MN assisted micro-particles delivery is developed. The model mimics the acceleration, separation and deceleration stages of the operation of a gene gun (or experimental rig) aimed at delivering the micro-particles into tissues. The developed model is used to simulate the particle velocity and the trajectories of micro-particles while they penetrate into the target. The model mimics the deceleration stage to predict the linear trajectories of the micro-particles which randomly select the initial positions in the deceleration stage and enter into the target. The penetration depths of the micro-particles are analyzed in relation to a number of parameters, e.g., operating pressure, particle size, and MNs length. Results are validated with experimental results obtained from the previous work. The results also show that the particle penetration depth is increased from an increase of operating pressure, particle size and MN length. The presence of the pierced holes causes a surge in penetration distance.

© 2014 Elsevier Ltd. All rights reserved.

## 1. Introduction

Gene guns are aimed at delivering DNA loaded micro-particles into target tissues at high speed (Zhang et al., 2013a; O'Brien and Lummis, 2006; Yang et al., 2004; Lin, 2000). The penetration depths of the micro-particles are typically greater than the stratum corneum, i.e., the top layer of skin (Yager et al., 2013; Kendall et al., 2004a, 2004b; Mitchell et al., 2003; Chen et al., 2002; Quinlan et al., 2001). To understand various features of the micro-particles delivery and evaluate achievable performance from the gene guns, mathematical models are often developed which aim to simulate

the micro-particles transfer process for specific gene delivery system. For example, Liu (2006) has focused on simulating the velocity distribution in the converging (conical) section of a venturi system developed for a gene gun, namely, the Powderject system (Bellhouse et al., 1994, 2003, 2006). The particle velocity has been simulated based on a balance between the inertia of micro-particles and other forces acting on the particles. Zhang et al. (2007) have used the programming platform MATrix LABoratory (MATLAB, the MathWorks Inc., Natick, USA; Shampine and Reichelt, 1997) to simulate three different stages of the particle delivery from a gene gun, namely, acceleration, separation and deceleration stages. In this work, the particle velocity have been analyzed on the basis of Newton's second law in the acceleration stage, energy conservation is applied to describe the separation of micro-carriers into micro-particles in the separation

\* Corresponding author. Tel.: +44 150 922 2509.

E-mail address: [d.b.das@lboro.ac.uk](mailto:d.b.das@lboro.ac.uk) (D.B. Das).

stage, and Stock's law is used to model the micro-particles penetration in the deceleration stage. Soliman et al. (2011) have used a commercial turbo-machinery flow simulator, namely, FINE™/Turbo (NUMECA International, Brussels, Belgium) to simulate the behaviour of gas and particle flow in a supersonic core jet in a gene gun. This work has used Newton's second law to determine the penetration depths of micro-particles in the skin. As discussed below, a number of other studies have shown that the penetration depths of micro-particles depend on the momentums of the particles which again depend on the particle size, density and velocity.

As well known, human skin is a major component of the body that must be considered in the study of micro-particles penetration. The skin helps to prevent the entry of foreign substances into the body (Holbrook and Odland, 1974; Scheuplein and Blank, 1971). It also provides a great resistance to the moving micro-particles during a particle delivery process. The skin consists of three main layers, which are the stratum corneum (SC), viable epidermis (VE) and the dermis (Parker, 1991; Phipps et al., 1988). On average the stratum corneum is between 10 and 20  $\mu\text{m}$  thick (Holbrook and Odland, 1974) which may vary in different regions of the body and amongst different groups of people. The thickness of the epidermis also varies in different regions of the body but it has been reported to have an average thickness of 20 to 100  $\mu\text{m}$  (Matteucci et al., 2009; Schaefer and Redelmeier, 1996). In addition, the thickness of the dermis varies between 1.5 and 3 mm (Lambert and Laurent, 2008) and especially on the back it can be up to 4 mm thick (Rushmer et al., 1966). The VE of the skin is the target layer for of DNA vaccination for previous needle free gene gun systems.

In a recent study, it has been shown that the penetration depths of micro-particles could be improved further to the dermis layer based on the use of microneedles (MNs) by creating holes on the target which allow a percentage of micro-particles penetrate through to achieve the purpose of improved penetration depth (Zhang et al., 2013b). MN arrays are minimally invasive systems that bypass the outer layer of skin, namely the *stratum corneum*, to achieve increased transdermal drug delivery (e.g., Olatunji and Das, 2011; Donnelly et al., 2012; Nayak et al., 2014; Olatunji et al., 2013; Cheung et al., 2014). MNs are broadly classified into two categories, namely, solid and hollow (e.g., Al-Qallaf et al., 2009; Olatunji and Das, 2010; Olatunji et al., 2012; Nayak and Das, 2013; Han and Das, 2013; Zhang et al., 2013a, 2013b; Olatunji et al., 2014). Using MNs and gene gun mimicking experimental rig (Fig. 1), Zhang et al. (2013b) have shown that pellets bound with

40 mg/ml concentration of Polyvinylpyrrolidone (PVP) concentration yield approximately 70% of passage percentage of a pellet mass with good control on the size distribution of separated micro-particles using a mesh of 178  $\mu\text{m}$  pore size. Solid micro-needles were used by Zhang et al. (2013b) to create pores/holes in the target tissue which remain for sufficiently long time after removing the MN. Within that time, micro-particles can be fired in the same tissue. It has been shown that a number of micro-particles can penetrate into the tissue via the holes while other micro-particles may be stopped from penetrating into the target by the non-porous (i.e., without MNs created holes) area of the tissue. The micro-particles transfer process of this system is divided into three stages, which are the acceleration, separation and deceleration stages. For the acceleration stage, a ground slide carries a pellet of micro-particles which are accelerated together to a desired speed by high pressure compressed air. In the separation stage, the pellet will be released from the ground slide after it reaches a stopping wall in a barrel; thereby it separates into micro-particles by a stopping screen with high speed. For the deceleration stage, the separated micro-particles spray forward, penetrate into the target via the holes made by solid micro-needle and stop inside the target.

Zhang et al. (2014a) have shown that the penetration depth of stainless steel micro-particles is enhanced in a skin mimicking agarose gel by using MNs. The work uses an agarose powder to prepare an agarose gel of a specific concentration (2.65 g/ml) to mimic the porcine skin based on its viscoelastic properties. This skin mimicking agarose gel is considered as a target instead of human skin to analyze the penetration depth of stainless steel micro-particles in relation to the operating pressure, particle size and MN length due to their homogeneity and transparency provide a good environment to observe the penetration by a digital optical microscope. The penetration depth of micro-particles in the gel is analyzed by an image processing software, namely, ImageJ (National Institutes of Health, Maryland, USA) (ImageJ, 2013). Zhang et al. (2014a, 2014b) show that the penetration depth increases with an increase of operating pressure, particle size and MN length. Especially, the high-speed micro-particles penetrate further into the target via the pierced holes which are created by MNs. However, the maximum penetration depth depends on the MN length which makes different lengths of holes on the target.

In order to further understand the characteristics of MNs assisted micro-particles delivery from gene guns, the present

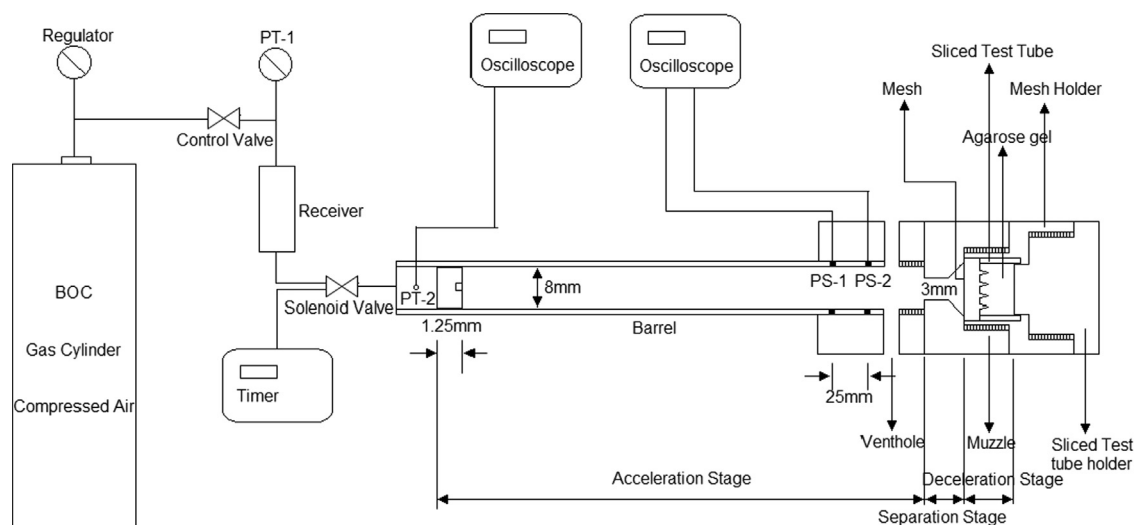


Fig. 1. A schematic diagram of the experimental rig for MN assisted micro-particles delivery (Zhang et al., 2013b).

study aims to develop a mathematical model of the process (Fig. 1) for delivering the micro-particles into a target. In particular this paper aims to simulate the penetration depths of the micro-particles. From an experimental point of view, the micro-particles are compressed into a cylinder pellet, loaded into a ground slide, and accelerated by pressurized air. Thus, the velocity of the pellet is defined to be equal to the velocity of the ground slide at the end of the barrel for this set up. The pellet is broken up into separated micro-particles which pass through a mesh. As expected, the velocities of the separated micro-particles decrease due to energy loss from the impaction and passage through the mesh.

In this paper, the mathematical formulation and its experimental validation are presented. The velocity of the micro-particles is simulated as it is one of the most important variables that determine penetration depth of the micro-particles in the deceleration stage. Furthermore, the model is formulated to mimic the acceleration, separation and deceleration stages of MNs assisted micro-particles delivery where the governing equations are solved using MATLAB (Version R2012b). It quantifies the effect of operating pressure on the velocity of the ground slide and compares the results with previous experimental data obtained by Zhang et al. (2013b) to verify the acceleration stage of the model. In addition, the trajectories of the micro-particles in the deceleration stage are simulated to determine the routes of the micro-particles and distribution of the micro-particles in the three layers of skin. The developed model is used to study the penetration depth of micro-particles in relation to operating pressure, particle size and MN length and these are compared with a selection of experimental results for the experimental validation. Please note that the paper is focused on modelling the micro-particle delivery process. The issues related to the loading of genes on these particles and subsequent gene transfection in a target cells are not discussed in this paper.

## 2. Methodology

### 2.1. Governing equations for micro-particles transport in various stages

As discussed earlier, the MNs assisted micro-particles delivery process consists of acceleration, separation and deceleration stages (Zhang et al., 2013a, 2013b, 2014a, 2014b). Brief operation principles of each stage and the corresponding governing equations that have been used to quantify the process are presented in the following sections.

#### 2.1.1. Acceleration stage

Acceleration stage uses a compressed gas as a driving force to accelerate the ground slide to a certain velocity which is controlled by the operating pressure in the receiver (see Fig. 1). A compressed gas (air in this case) is released from a gas cylinder and stored in the receiver (Zhang et al., 2013b). The pressure inside the receiver is detected by a sensitive pressure transducer. Before the solenoid valve of the system is opened, the initial volume and pressure inside the receiver are  $V_1$  and  $P_1$ . After the valve is opened, the gas expands and accelerates the ground slide. The volume of air increases to  $V_2$  and the pressure decreases to  $P_2$ . Assuming that the gas expands adiabatically, we can apply the Boyle's law (Webster, 1995) to obtain:

$$P_1 V_1^\gamma = P_2 (V_1 + V_2)^\gamma \quad (1)$$

where  $\gamma$  is the heat capacity ratio. This process defines gas as a fluid where  $\gamma = 1.4$  for diatomic gas and  $\gamma = 1.6$  for a monatomic gas.

In the acceleration stage, only air does work on the ground slide. The work done by the gas is:

$$\int_0^L P_2 \pi R^2 dl = E \quad (2)$$

where  $L$  is the length of the acceleration stage and  $R$  is the radius of the ground slide.

We define the final velocity of ground slide before reaching the stopping wall as  $u$ , and the mass of ground slide with the pellet as  $M$ . The kinetic energy of the ground slide is therefore given as:

$$E = \frac{1}{2} M u^2 \quad (3)$$

The sliding friction of the ground slide travelling in the channel is neglected in this formulation. Based on the law of conservation of energy, the velocity of the ground slide is given as:

$$u = \sqrt{\frac{2 P_1 V_1^\gamma [(V_1 + \pi R^2 L)^{1-\gamma} - (V_1)^{1-\gamma}]}{M(1-\gamma)}} \quad (4)$$

#### 2.1.2. Separation stage

In the separation stage, the compressed air is released from the vent hole (see Fig. 1) and the ground slide blocks the gas from flowing into the deceleration stage (Zhang et al., 2013a, 2013b). Further, the pellet is broken up and separated into individual micro-particles by a mesh which then move across the mesh into the deceleration stage. In this process, the initial velocity of the pellet is equal to  $u$  which is the velocity of the ground slide. The pellet may lose some energy due to its impact on the mesh which separates it into individual micro-particles. Assuming that the energy loss is  $x$  in this process, the process is described based on the law of conservation of energy and given as:

$$\frac{1}{2} n m u_1^2 = (1-x) \times \frac{1}{2} m_p u^2 \quad (5)$$

where  $n$  is the number of micro-particles in the pellet;  $m$  is the mass of a single micro-particle;  $u_1$  is the velocity of micro-particles after passing through the stopping screen and  $m_p$  is the mass of the pellet which can be described as  $m_p = nm$

The rearranged Eq. (5) gives:

$$\sqrt{1-x} \times u = u_1 \quad (6)$$

#### 2.1.3. Deceleration stage

The deceleration stage can be separated into two parts. In the first part, the particle travels between the mesh and the target. There is a gap between the mesh and target which allows spraying of the micro-particles on a large-area of the target tissue. Thus, the air drag force acting on the separated micro-particles should be considered in this process. The second step involves modelling the process of the particle penetration in the skin, which requires consideration of the resistance force from the skin on the micro-particles delivery. The micro-particles need to breach the SC and pierce the subsequent layers, e.g., the epidermis layer. The detailed mathematical principles of these two steps are explained in Sections 2.1.3.1 and 2.1.3.2.

The trajectories of the micro-particles in the deceleration stage are simulated in two dimensions (2D). The initial positions and moving directions of high-speed micro-particles are randomly chosen from the beginning in the first step of the deceleration stage. The motion is considered to be linear but varying in velocity of the particles due to the effects of drag force on the particles. The particles are allowed to impact on the boundary of the gap between the mesh and skin. We define that these impacts are elastic collisions and the particles rebound on the boundary in the

model. The detailed physical-mathematical principle of the micro-particle trajectories are discussed in Section 2.1.3.3.

**2.1.3.1. Micro-particles travel in the gap between mesh and skin.** The separated particles decelerate in air before hitting the target (Zhang et al., 2013a, 2013b). This process is described by the following energy balance equation:

$$E_2 + E_{sfe} + E_d = \frac{1}{2}mu_1^2 \quad (7)$$

where  $E_2$  is the final kinetic energy of the separated micro-particle.  $E_{sfe}$  is the surface free energy of the pellet and  $E_d$  is the energy lost due to the frictional drag force from the micro-particles in the air.

The frictional drag force on a micro-particle in the air is given as:

$$F_d = \frac{1}{2}\rho u_2^2 C_d A_p \quad (8)$$

where  $F_d$  is the force of drag,  $\rho$  is the density of air,  $A_p$  is the projected cross-sectional area of the separated micro-particle,  $C_d$  is the air drag coefficient and  $u_2$  is the velocity of the separated particle in the space between mesh and target.

The energy loss due to the drag force is given as:

$$E_d = \int_0^{L_1} F_d dl \quad (9)$$

After differentiating the energy loss  $E_d$  with the distance  $l$  we obtain:

$$F_d = \frac{dE_d}{dl} \quad (10)$$

where  $l$  is the gap between the mesh and target.

The final kinetic energy of the separated particles before they hit the target is given as:

$$E_2 = \frac{1}{2}mu_2^2 \quad (11)$$

Based on Eqs. (8) and (10), the relationship between the particle velocity and travel distance is given as

$$-mu_2 \frac{du_2}{dl} = \frac{1}{2}\rho u_2^2 C_d A_p = F_d \quad (12)$$

The drag coefficient  $C_d$  in Eq. (12) is an important parameter in the modelling of gas and particle interactions. This coefficient is a function of the particle Reynolds number (Re), which depends on the gas viscosity ( $\mu$ ) and density ( $\rho$ ), particle diameter ( $d$ ), and relative velocity ( $u_2$ ). For the purpose of this paper, the Reynolds number is defined as:

$$Re = \frac{\rho u_2 d}{\mu} \quad (13)$$

The relationships between  $C_d$  and Reynolds number, as used in this work, are shown in Appendix A.

**2.1.3.2. Micro-particles penetration in the target tissue.** The particle deceleration in the target skin has the same principle with the particle travel in the air. In the deceleration stage, the separated micro-particles are resisted by the tissue and their velocities are slowed down. Based on the law of conservation of energy, the drag force can be expressed as:

$$f_d = -m \frac{du_d}{dt} \quad (14)$$

where  $f_d$  is the drag force for the micro-particles,  $u_d$  is the velocity of separated micro-particles in the tissue.

For the penetration in the target, various studies have adopted that the resistant force on the micro-particle is separated into three components, namely, yield force ( $F_y$ ), frictional resistive force ( $F_f$ ) and resistive inertial force of target material ( $F_i$ ) (Soliman et al., 2011; Liu, 2007; Mitchell et al., 2003; Kendall et al., 2001; Dehn, 1987). In consistent with these previous studies, we adopt the following the force balance equation:

$$m \frac{du_d}{dt} = -(F_i + F_f + F_y) \quad (15)$$

The equation for each component of the resistant force is as shown below:

$$F_i = 6\pi\mu_t r_p u_d \quad (16)$$

$$F_f = \frac{1}{2}\rho_t A_p u_d^2 \quad (17)$$

$$F_y = 3A_p \sigma_y \quad (18)$$

where  $\mu_t$  is the viscosity of the target,  $r_p$  is the radius of the micro-particle,  $\rho_t$  is the density of the target and  $\sigma_y$  is the yield stress of the target.

**2.1.3.3. The mathematical-physical principle and determination of micro-particle trajectory in deceleration stage.** To determine the trajectory of the micro-particles, the mathematical statement is formulated in two dimensions. Depending on the velocity, size of particle, etc., other important features of this is the possibility of different angles and positions of particle entrance which have direct implication on the velocity of the micro-particles. The air in the deceleration stage might move forward when the high pressure gas pushes the ground slide forward. Although the ground slide can stop the gas from entering the deceleration stage, the air flow still happens in the front of the ground slide and causes pressure drop in the deceleration stage. Hence, the axial gas pressure drop is greater than that in the radial direction, i.e.

$$\frac{dP_z}{dz} > \frac{dP_r}{dr}$$

As  $(dP_z/dz) > (dP_r/dr)$ , the axial ( $z$ ) velocity component is greater than the radial ( $r$ ) component. Further, the velocity of the separated particle in the space between mesh and target is  $u_2$ , and the initial velocity is equal to  $u_1$ .

Therefore

$$u_2^2 = u_z^2 + u_r^2 \quad (19)$$

We define that the radial velocity component as  $k$  percentage of the axial component.

Therefore

$$u_r = k u_z \quad (20)$$

In our case,  $k$  is defined to be 0.2. The air in the holes of microneedles may flow when the high pressure gas pushes the ground slide along in the system (i.e., the barrel). Although, the ground slide can stop the gas from entering the deceleration stage, the air flow still happens in front of the ground slide and causes changes in pressure drop in the deceleration stage. In this case, the axial velocity component is greater than the radial component and, therefore, the  $k$  value should be low so that it practically imposes the above condition in the simulations. In reality, it is not easy to identify or directly measure the  $k$  values. Therefore,



we have adopted an indirect approach to ascertain the value in our case. For this purpose, we have chosen three different  $k$  values, i.e., 0.1, 0.2 and 0.3, and determined the ground slide velocity for each case. As we have the experimental data for the velocity as well, we compared the experimentally determined data to the simulated results. The results show that at these low values  $k$ , the ground slide velocity is not significantly affected by  $k$  values. More importantly, the results for the  $k$  value of 0.2 seem to match slightly better with the experimental results as compared to the other  $k$  values. On these bases, we have chosen a  $k$  value of 0.2 for all our simulations in this work.

**2.1.3.4. Micro-particle travel between mesh and target.** In the first part of the deceleration stage, the air drag force is presented in Eq. (8). According to Newton's second law:

$$F_d = ma = m \frac{du_2}{dt} \quad (21)$$

Substitution of Eq. (8) into Eq. (21) provides:

$$m \frac{du_2}{dt} = \frac{1}{2} \rho u_d^2 C_d A_p \quad (22)$$

For axial component, we have

$$m \frac{du_r}{dt} = \frac{1}{2} C_d \rho u_d u_x A_p \quad (23)$$

For radial component

$$m \frac{du_z}{dt} = \frac{1}{2} C_d \rho u_d u_y A_p \quad (24)$$

At the same time, the radial displacement component is:

$$\frac{dl_r}{dt} = u_r \quad (25)$$

The axial displacement component is:

$$\frac{dl_z}{dt} = u_z \quad (26)$$

The program uses an *if* statement to define the axial displacement component of the micro-particle is smaller than the space between the mesh and target or the radial displacement

component is smaller than  $l_y$ , the particle will impact on the walls before entering the skin.

**2.1.3.5. Micro-particle penetration in skin.** Once the micro-particles reach the surface of the target tissue, an increased resistance from the target prevents those micro-particles to move forward. The initial velocities of the micro-particles in axial and radial components equal the velocity at the end of the first step of deceleration stage. The following velocity change of the micro-particles is calculated based on the Newton second law and it is shown in Eq. (27) which is obtained from Eq. (15):

$$m \frac{du_d}{dt} = \frac{1}{2} \rho u_d^2 A_p + 3A_p \sigma_y + 6\pi \mu_t r_p u_d \quad (27)$$

For the axial component of Eq. (27), we have

$$m \frac{du_r}{dt} = \frac{1}{2} \rho u_d u_r A_p + 3A_p \sigma_y \frac{u_r}{u_d} + 6\pi \mu_t r_p u_r \quad (28)$$

On the other hand, the radial component of Eq. (27) is

$$m \frac{du_z}{dt} = \frac{1}{2} C_d \rho u_d u_y A_p + 3A_p \sigma_y \frac{u_z}{u_d} + 6\pi \mu_t r_p u_z \quad (29)$$

In the program, we have used an *if* statement to define the location of micro-particle. If the axial displacement component of a micro-particle is larger than the space between the mesh and target, and the radial displacement component is located at a space between two holes, the particle will pierce into the target skin. If the axial displacement component of the micro-particle is larger than the space between the mesh and target and the radial displacement component is located at a hole area created by the MN, the particle is defined to be delivered in a hole. Thus, a micro-particle is defined to travel forward in the hole, penetrate into the skin, and achieve a further penetration depth inside skin. The model behaviour is explained in Section 2.3 in detail.

**2.1.3.6. Quantitative description of the events involving micro-particle rebound between mesh and target.** In the first step of deceleration stage, the micro-particles may impact on the boundary of the gap between the mesh and target skin. We define that the particles impact on the boundary of the gap between the mesh and skin is an elastic collision, see Fig. 2.

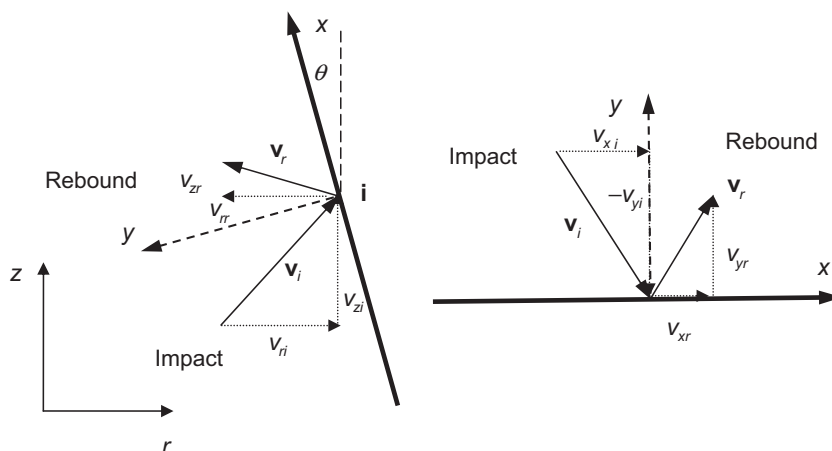


Fig. 2. The trajectory of particle impact on a planar wall.

The coordinates of radial and axial velocity components at a point on  $(x,y)$  axes are defined as  $(V_x, V_y)$ . From Fig. 2, it can be seen that in order to change from  $(x,y)$  axes to  $(r,z)$  axes, a rotation through  $((\pi/2)+\theta)$  is required. The new coordinates of the tangential and normal velocity components of that point are  $(V_r, V_z)$  on  $(r, z)$  axes. Using the standard matrix rules (Eberly, 2002) to perform the axes- rotation of the velocity vectors gives

$$\begin{pmatrix} V_r \\ V_z \end{pmatrix} = \begin{pmatrix} \cos(\frac{\pi}{2}+\theta) & -\sin(\frac{\pi}{2}+\theta) \\ \sin(\frac{\pi}{2}+\theta) & \cos(\frac{\pi}{2}+\theta) \end{pmatrix} \begin{pmatrix} V_x \\ V_y \end{pmatrix} \\ = \begin{pmatrix} -\sin\theta & -\cos\theta \\ \cos\theta & -\sin\theta \end{pmatrix} \begin{pmatrix} V_x \\ V_y \end{pmatrix} \quad (30)$$

When inverted, Eq. (30) gives

$$\begin{pmatrix} V_x \\ V_y \end{pmatrix} = \begin{pmatrix} -\sin\theta & \cos\theta \\ -\cos\theta & -\sin\theta \end{pmatrix} \begin{pmatrix} V_r \\ V_z \end{pmatrix} \quad (31)$$

Eq. (31) therefore suggests that for the velocity on impact, the tangential and normal velocity components on the impact plane are

$$\begin{aligned} V_{xi} &= -V_{ri} \sin\theta + V_{zi} \cos\theta \\ V_{yi} &= -V_{ri} \cos\theta - V_{zi} \sin\theta \end{aligned} \quad (32)$$

$$\begin{aligned} V_{xr} &= e_t V_{xi} \\ V_{yr} &= -e_n V_{yi} \end{aligned} \quad (33)$$

Hence, rotating back through  $((\pi/2)+\theta)$ , using Eq. (30), to get the radial and axial velocity components on rebound provide:

$$\begin{aligned} V_{rr} &= -e_t \sin\theta (-V_{ri} \sin\theta + V_{zi} \cos\theta) \\ &\quad + e_n \cos\theta (-V_{ri} \cos\theta - V_{zi} \sin\theta) \\ V_{zr} &= e_t \cos\theta (-V_{ri} \sin\theta + V_{zi} \cos\theta) \\ &\quad + e_n \sin\theta (-V_{ri} \cos\theta - V_{zi} \sin\theta) \end{aligned} \quad (34)$$

We define the collisions between micro-particles and the boundary of the gap between mesh and skin are elastic collision, and then the coefficient of restitution is equal to 1. It means that there is no energy lost due to the rebound; only the direction of motion has been changed Table 1.

## 2.2. Selection of modelling parameters

The impact velocity, particle size and density, target properties are defined as the major variables affecting the penetration depth. The layers of the skin are considered to mimic the human skin in

the model (see Fig. 3a). The skin is divided into two distinct macroscopic layers known as the dermis and the epidermis (Parker, 1991; Phipps et al., 1988). Stratum corneum is considered as a part of the epidermis layer. Therefore, the skin is considered to have three layers in the model, which are shown in Fig. 3b which is a magnified profile of a section of the model geometry shown in Fig. 3a. The thicknesses of the different skin layers differ which are listed in Table 2. The viscosity of each layer is treated as the same in the model. Previously, Zhang et al. (2014a) have analysed the viscosity of the porcine skin using a rotational viscometer, which will be used as a replacement for human skin in the model and shown in Table 4. For example, the density of the stratum corneum and viable epidermis are defined as 1.5 and 1.15 g/cm<sup>3</sup>, respectively, in consistent with the results of Duck (1990). Wildnauer et al. (1971) have shown that the yield stress of stratum corneum range from 3.2 to 22.5 MPa, which have been obtained from the measurements of stress-strain characteristics of the human stratum corneum samples.

In order to investigate the MN effect on the penetration depth, an in-house fabricated MN, Adminpatch MN 1500 and 1200 are (nanoBioSciences limited liability company, Sunnyvale, CA, USA) chosen for both model and experiments. The detailed characterizations of each MN are shown in Fig. 4 and explained in Table 3. Zhang et al. (2014a) have chosen Adminpatch MN 1500 to analyse the MNs assisted micro-particles delivery and show that the lengths of pierced holes vary after the removal of the MNs. But, the length of the pierced holes are considered uniform in the model and presented in Table 4. It is worth mentioning that the lengths of the pierced holes are from a study of the insertion of MN in a skin mimicking agarose gel (0.0265 g/ml of agarose), which has been obtained in a previous work (Zhang et al., 2014a). McAllister et al. (2003) have assumed that after the removal of the MNs the surface area of the hole shrink to 60 percent of that the MNs which originally create the holes. In consistent with McAllister et al.(2003), the hole width is considered to be 60% of the width/radius of the MN (Table 4) at the time the micro-particles are delivered. The details can be shown in Fig. 3a, which presents the pierced holes as uniform cones.

The relevant simulation parameters of the proposed gene gun system are obtained from an experimental rig, which include the mass of the ground slide with pellet, volume of receiver, barrel length and radius and space between mesh and target (skin). Spherical and irregular stainless steel particles of 18 and 30  $\mu$ m average diameters are chosen to study the effects of particle size on the penetration depth for both the model and experiment. The details of the relevant parameters used in the model are listed in Table 4.

## 2.3. Solving governing equations

The governing equations for modelling the MNs assisted micro-particles delivery are solved using MATLAB (Version R2012b). MATLAB is a powerful programming software for computing and data processing and visualisation. For our case, we have used MATLAB's in-built programming language to simulate the particle delivery process in each stage. The presented model consists of a main program to explain the overall process of the micro-particles delivery, several function programs to input the integration of the required mathematical equations, event programs to define the event locators of the rebound and impact points. All constant variables (e.g. skin properties, particle properties) are included as declared global variables at the start of the program with comments in the main program for the following simulation (see Tables 2–4). The acceleration stage is analysed in one-dimensional using Eq. (4) in the main program to predict the velocity from the beginning to the end of the barrel at various pressures. The

**Table 1**  
The meaning of each variable in Fig. 2.

Variables	Description
$V_i$	The velocity on impact
$V_{ri}$	The radial velocity component on impact
$V_{zi}$	The axial velocity component on impact
$V_r$	The velocity on rebound
$V_{rr}$	The radial velocity component on rebound
$V_{zr}$	The axial velocity component on rebound
$\theta$	The angle of boundary of the gap between mesh and skin
$I$	The impact point
$V_{xi}$	The tangential velocity component on impact
$V_{yi}$	The normal velocity component on impact
$V_{xr}$	The tangential velocity on rebound
$V_{yr}$	The normal velocity on rebound

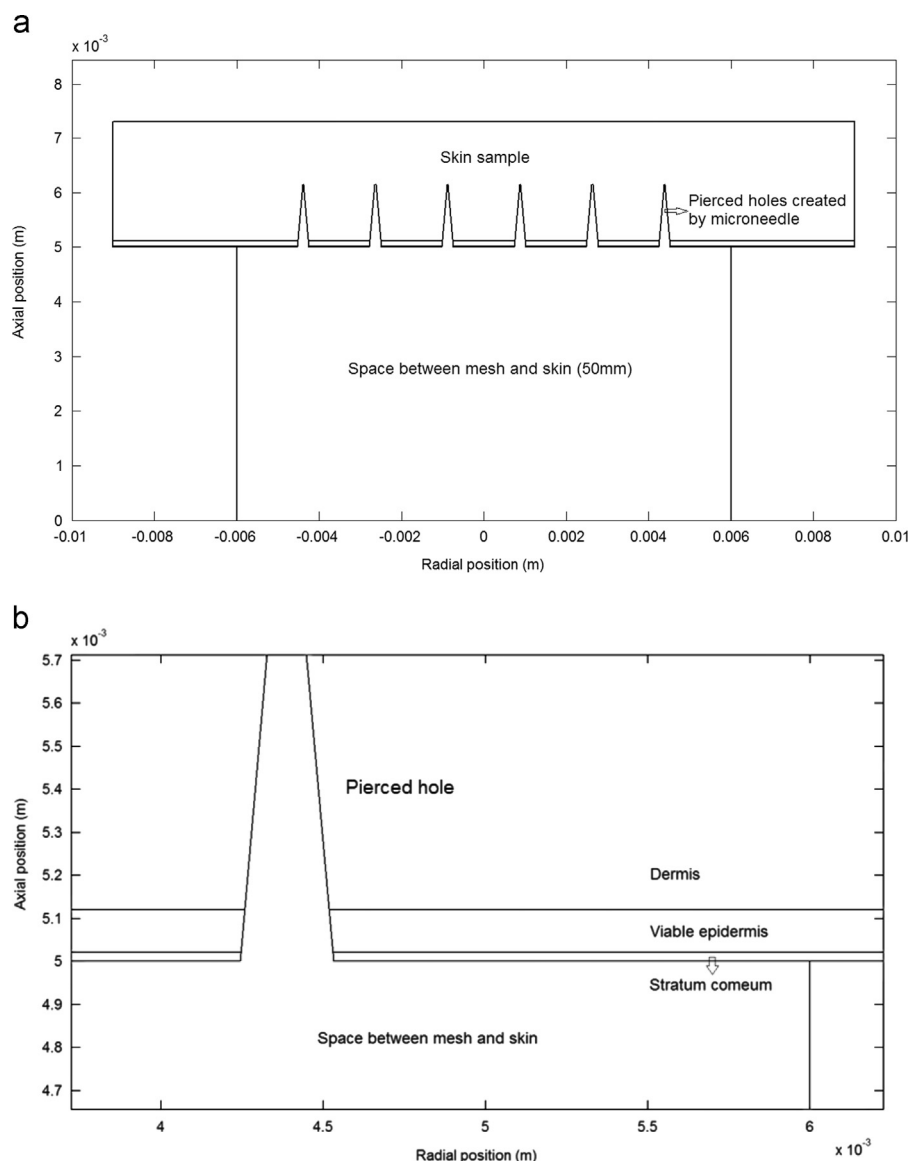


Fig. 3. Structure of the deceleration stage (Adminpatch 1500): (a) the overall view of the deceleration stage, (b) the zooming view to show the skin layers.

Table 2

Skin properties used in the model.

Parameter	Value	Refs.
Thickness of VE, $T_{ve}$ (m)	0.0001	Holbrook and Odland (1974)
Thickness of SC, $T_{sc}$ (m)	0.00002	Matteucci et al. (2009)
Yield stress of SC, $Y_{sc}$ (MPa)	3.2–22.5	Schaefer and Redelmeier (1996)
Density of SC, $\rho_{sc}$ (g/cm <sup>3</sup> )	1.5	Wildnauer et al. (1971)
Density of VE, $\rho_{ve}$ (g/cm <sup>3</sup> )	1.15	Duck (1990)
Yield stress of VE, $Y_{ve}$ (MPa)	2.2	Duck (1990)
Viscosity of skin, $\mu_t$ (Pas)	19.6	Kishino and Yanagida (1988)
		Zhang et al. (2014a)

separation stage is implemented using Eq. (6) in the main programme to define the energy loss of micro-particles during separation stage and then to calculate the velocity of micro-particles after the passage through the mesh.

The presented model is focused on determining the trajectories of micro-particles in the deceleration stage. Firstly, the initial velocity of separated micro-particles in the deceleration stage ( $u_2$ ) is defined to be equal to  $u_1$  which is the final velocity of the separated micro-particles after passing through the mesh.

The velocity of the separated micro-particles is then analysed in relation to time. After that a two dimensional figure corresponded to the structure of the deceleration stage is prepared based on the size of experimental set up as shown in Fig. 3. The initial position and moving direction of high-speed micro-particles are randomly chosen from the beginning in the first step of the deceleration stage to mimic the condition of micro-particles passage through the mesh. The motion is considered to be linear but varying in velocity of the particles due to the effect of drag force. However, the mathematical equations used to determine the particle velocity are implemented in a separate function. An *if* statement is used to determine the selection of equations to calculate the particle velocity at different positions. This program is implemented to the main program by considering the condition of the function program (stiff/non-stiff) to choose a suitable *ode* solver to determine the velocity changing of micro-particles and plot the trajectories in the pre-plotted figure (Fig. 3). The penetration depth of micro-particles in the skin is obtained from the figure. In addition, Eqs. (12) and (15) are solved using a separately function program and implemented into the main program to predict the penetration depth of micro-particles with/without using MNs in one-dimensional simulation. A *for* statement is used

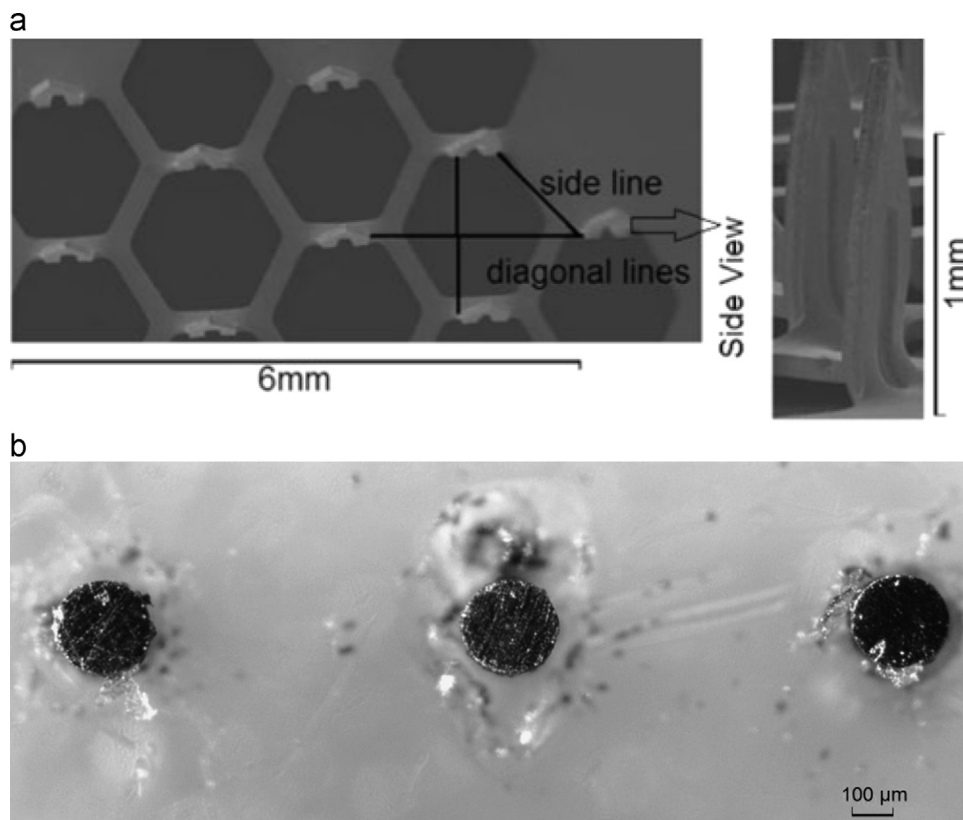


Fig. 4. The image of MN arrays: (a) Adminpatch 1200, (b) in-house fabricated MN arrays.

**Table 3**  
The characterizations of the MN array (Zhang et al., 2013b).

Name	Parameters	Value ( $\mu\text{m}$ )
Adminpatch MN 1500	Length	1500
	Width	480
	Thickness	78
	Space between MNs	1546
Adminpatch MN 1200	Length	1200
	Width	480
	Thickness	78
	Space between MNs	1252
In-house fabricated MN	Length	750
	Diameter	250
	Space between MNs	500

**Table 4**  
Relevant constants used in the developed model.

Parameter	Value
Mass of ground slide with the pellet, $M$ (g)	1.25
Length of barrel, $L$ (m)	0.5
Radius of barrel/ground slide, $R$ (m)	0.00375
Volume of receiver, $V_1$ (L)	1
Space between mesh and skin, $L_1$ (m)	0.05
Density of stainless steel ( $\text{g}/\text{cm}^3$ )	8
Average Diameter of spherical stainless steel particle ( $\mu\text{m}$ )	18
Average Diameter of Irregular stainless steel particle ( $\mu\text{m}$ )	30
Viscosity of air, $\mu$ (Pas)	1.78
Length of pierced holes $L_p$ ( $\mu\text{m}$ ) Adminpatch 1500	1149
Adminpatch 1200	1048
In-house fabricated MN	656
Width of pierced holes $L_w$ ( $\mu\text{m}$ ) Adminpatch 1500	302
Adminpatch 1200	302
In-house fabricated MN	156

to repeat the same procedure to simulate a number of micro-particles trajectories in the program. However, the number of micro-particles is defined as a constant and inputted at the start of the main program.

Event program is used to define the impact points on the skin and the boundary of the gap between mesh and skin, and further to point out the end position of micro-particles inside the skin. Setting the events cause the solver to stop the integration when the micro-particles impact on the skin and the boundary of the gap between mesh and skin, and then restarts the integration corresponding to the continuous moving of a micro-particle. In addition, an event causes the solver to stop the integration when the velocity of micro-particles is less than  $10^{-10}$  m/s. This event program is implemented in the main program to predict the events of micro-particles (e.g. impact on the boundary, penetrate into the skin) and show on the particle trajectories.

### 3. Results and discussions

#### 3.1. Acceleration stage

The micro-particle velocity is a key variable in the micro-needle assisted micro-particles delivery process which is simulated and discussed in this section. As mentioned earlier, the developed mathematical model is built to simulate the acceleration stage of this process where a number of variables are considered such as the mass of the ground slide (including the pellet), volume of the gas receiver and, barrel length and diameter. The relevant constants are listed in Table 4.

The operating pressure is another key variable in the model which affects the velocity of the ground slide. The principle of modelling the acceleration stage is explained in Section 2.1.1. Indeed the model results show that the operating pressure has a



significant effect on the ground slide velocity (Fig. 5). As can be seen, an increase in the operating pressure causes an increased ground slide velocity. The velocities of ground slide reach 85.5, 102.2, 125.1, 138.3 and 144.5 m/s at 2.1, 3, 4.5, 5.5 and 6 bar pressures, respectively.

Zhang et al. (2013b) have used a pair of photoelectric sensors to test the velocity of the ground slide in a set of experiments. A comparison is made between the results from the developed model and Zhang et al. (2014a)'s experiments which are shown in Fig. 6. As can be seen, both sets of results compare well at the chosen pressures. The velocity increases from an increase of operating pressure due to an increased kinetic energy of the ground slide. This set of results provides the confidence that the developed model is suitable for modelling the acceleration stage of the micro-needle assisted micro-particles delivery.

It is seen that the predicted velocity is comparable with the velocity of the ground slide based gene gun system, e.g. light gas gun (Crozier and Hume, 1957; Mitchell et al., 2003) which can accelerate the micro-particles to velocities of 170, 250, 330 m/s at 20, 40 and 60 bar pressure. In this work the ground slide is operated at 6 bar which shows that the velocity is slightly different with the LGG operated at 20 bar pressure. However, the velocity is much slower if it is compared with that of other gene gun systems, e.g. contoured shock tube (Truong et al., 2006; Mitchell et al., 2003), converging-diverging nozzle (Kendall et al., 2004a) and

conical nozzle (Quinlan et al., 2001). The micro-particles normally can achieve a supersonic speed based on a needle free powder injection system, such as golden particle injector which may reach a velocity over than 600 m/s at 60 bar pressure using contoured shock tube (Liu, 2006; Mitchell et al., 2003). This is because the effects of the ground slide which slows down the particle velocity.

An insufficient velocity means that the micro-particles cannot reach the desired depth inside the target due to the insufficient momentum. As the operating pressure was limited in the experiments of Zhang et al. (2013b), the velocity of the ground slide is simulated to reach a velocity of 457 m/s at 6 MPa using the model, which is much higher than the velocity obtained from LGG. Zhang et al. (2013b) have shown that the velocity increases with a decrease in barrel diameter and ground slide mass. Therefore, the velocity can improve by changing those two objects in Zhang et al. (2013b)'s experimental set up if higher velocity is necessary. Furthermore, Zhang et al. (2014a) suggest that the penetration depth is maximized by using MNs. The MNs make up for the insufficient velocity of the micro-particles since the pierced holes created by MNs provide a positive effect on the penetration depths. This is explained more in Section 3.2.

### 3.2. Deceleration stage

#### 3.2.1. The trajectory of the micro-particles

Zhang et al. (2013b) have shown that a pellet can be separated into individual particles with a few agglomerates using a mesh which then can penetrate into the target. In this paper, the presented mathematical model is used to simulate the trajectories of stainless steel micro-particles of 30  $\mu\text{m}$  average diameter in the deceleration stage. As presented in Fig. 7a, the velocity of the micro-particles is represented by the coloured trajectory. It is found that the velocity variation is negligible before they reach the target as the effect of air drag force on the micro-particles is low. It is also found that the velocity reaches approximately 131 m/s at 5 bar operating pressure according to the results in the figure. In addition, the micro-particles rebound on the boundary of the gap between mesh and skin is clearly shown in Fig. 7a. However, the penetrations of micro-particles in the target are not visible in this figure.

In theory, the particle velocity must decrease fast after penetrating into the skin due to an increased resistance to its motion. The variation of the velocity is shown in more detail in Fig. 7b, which is obtained from zooming in a part of Fig. 7a. As can be seen, the micro-particles only penetrate slightly in the stratum corneum layer of skin. The detailed penetration depth refers to the results of dashed line in Fig. 8 (see the zoomed view of the axis), which shows that the stainless steel micro-particles of 30  $\mu\text{m}$  diameter only penetrate around 1.9  $\mu\text{m}$  inside the stratum corneum.

Fig. 7a also shows that a number of the micro-particles achieve a further penetration depth via the pierced holes. Some of them reaches the hole tip area as shown in Fig. 7c. The velocity is changed only slightly in the pierced holes and decrease fast after penetrating the dermis layer of the skin. The penetration depth of the micro-particles via the pierced holes is shown in Fig. 8 (see the zoom in view of the axis). As can be seen, the penetration depth of the micro-particles reaches 1151.1  $\mu\text{m}$  when Adminpatch MN 1500 is used. However, some particles cannot reach the holes tip and penetrate through the skin surface of the pierced holes to achieve a further depth inside the epidermis/dermis layer of the skin as shown in Fig. 7d.

Finally, delivery of an arbitrarily selected number of micro-particles, namely one hundred (100) micro-particles, has been simulated to determine the particle's final location in each layer of skin. As presented in Fig. 9, it shows that about 75% of micro-particles stop inside the stratum corneum, 2% is located within the

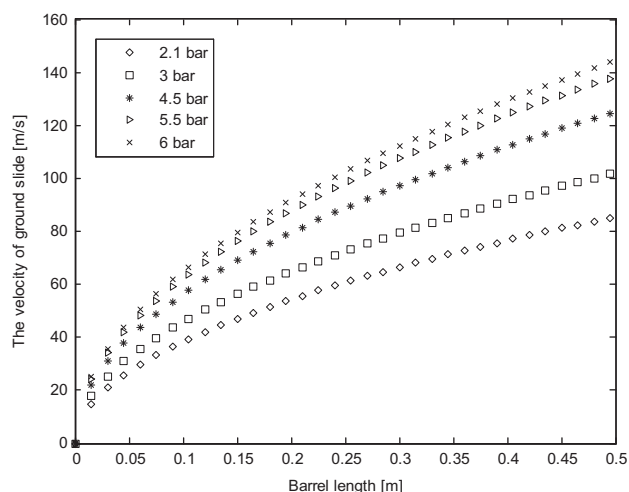


Fig. 5. Effect of the operating pressure on the ground slide velocity (modelling results).

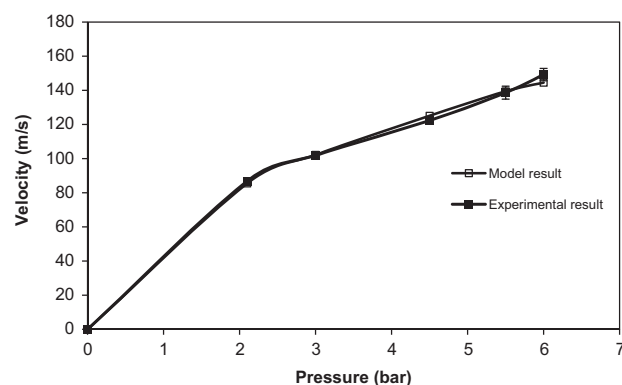
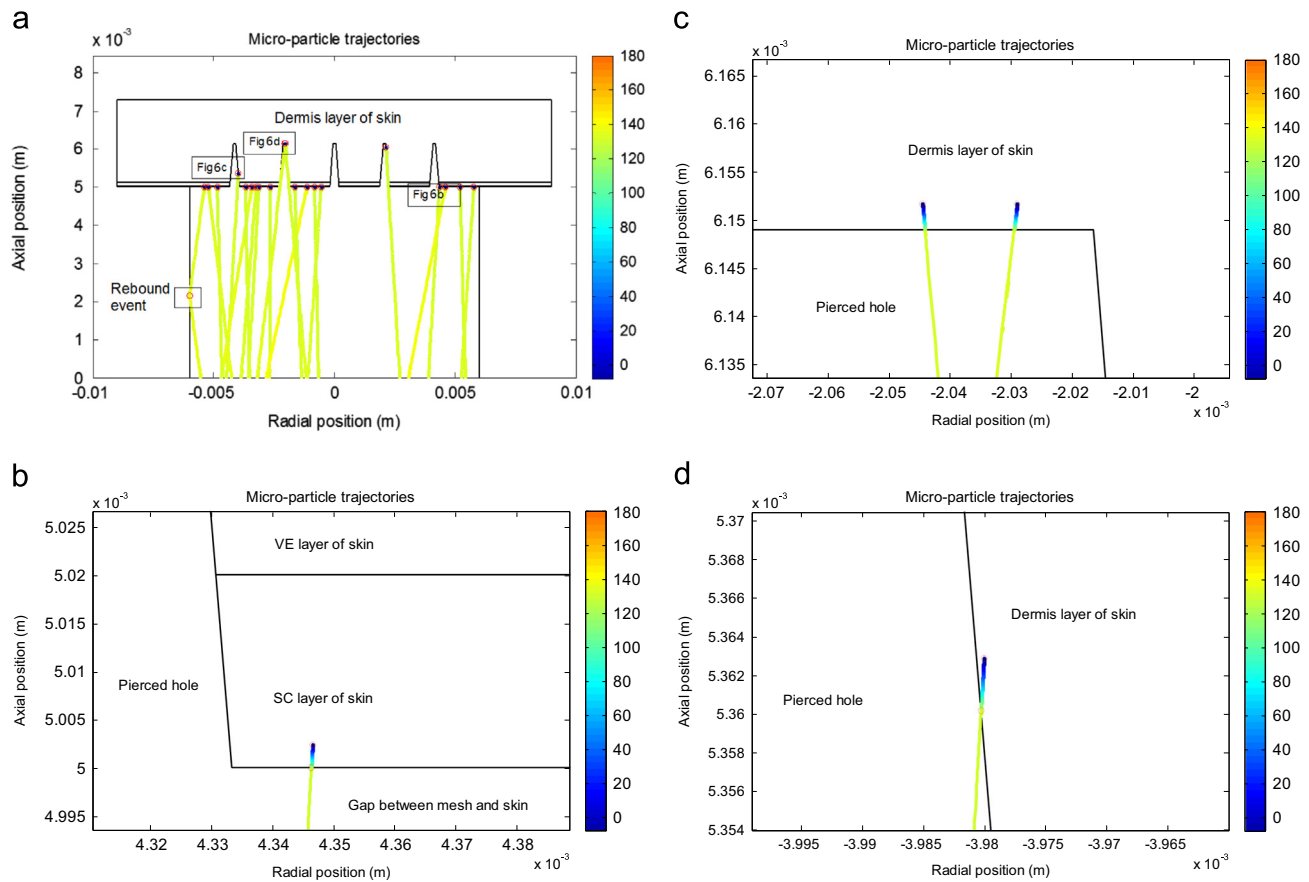
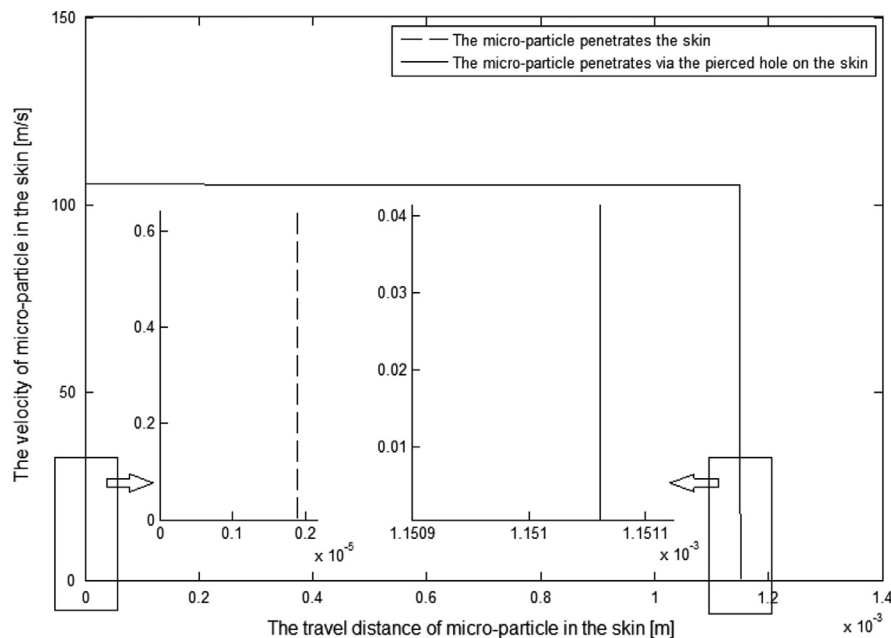


Fig. 6. Comparison of modelling (this work) and experimental (Zhang et al., 2013b) results of the ground slide velocity against the operating pressure. The experimental results in the figure are generated from three repeats of experiments.



**Fig. 7.** The trajectories of the micro-particles in the deceleration stage for the MN assisted micro-particles delivery: (a) The overall view of the micro-particles trajectories, (b) The particle penetration at the area without needle hole, (c) The particle penetration at the hole tip area inside skin (d) Particle penetrates into the side surface of the needle hole inside skin (stainless steel micro-particles of 30 diameter; pressure: 5 bar).



**Fig. 8.** The travel distance of micro-particles in the skin against the velocity.

epidermis layer, and 23% penetrates further into the dermis layer. In addition, the micro-particles stopped inside the epidermis or dermis layer are considered to penetrate through the pierced holes, which illustrate the use of the Adminpatch MN 1500

allowing approximately 25% of the micro-particles penetration in the skin via the pierced holes. The detailed effects of the MN length, particle size and operating pressure on the penetration depth are explained in the following sections.

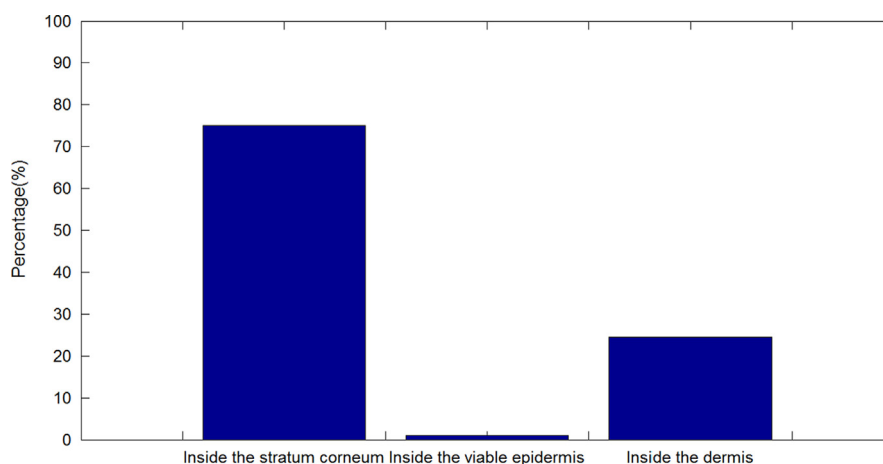


Fig. 9. The distribution of the micro-particles in different layers of skin.

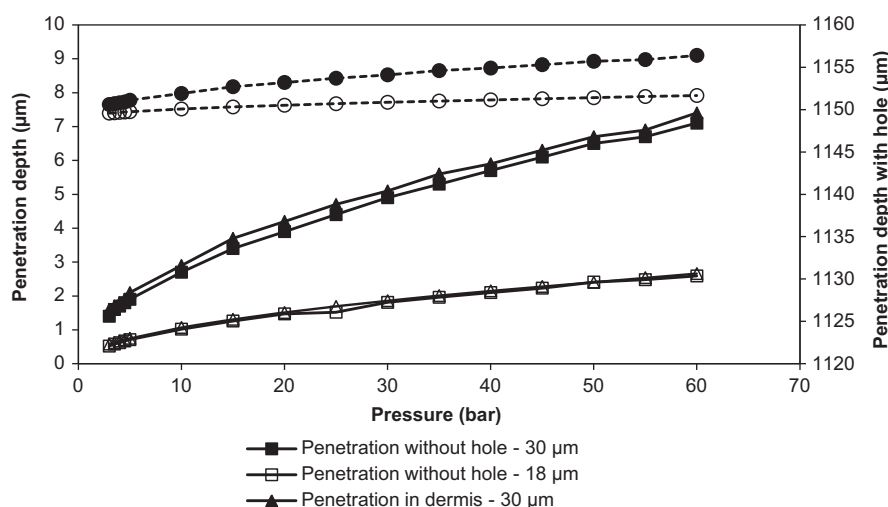


Fig. 10. The effect of the operating pressure on the penetration depth of the micro-particles in the skin (stainless steel micro-particles: 18 and 30 μm average diameters; MN: Adminpatch MN 1500; solid line: primary y axis; dashed line: secondary y axis).

### 3.2.2. Comparison with experimental results

As mentioned earlier, Zhang et al. (2013b) have used an agarose gel to mimic the skin on the basis of rheological properties using a rotational viscometer. The work shows that the rheology of 0.0265 g/ml concentration of agarose gel matches well with that of porcine skin, and this skin mimicking agarose gel is used as a target instead of human skin to analyse the penetration depth in relation to the operating pressure, particle size and needle length. The operating pressure is varied from 3 to 5 bar to accelerate biomedical grade stainless steel micro-particles of 18 and 30 μm average diameters to analyse the effect of the particle size and operating pressures on the penetration depths of the particle. Three different lengths of micro-needle arrays, which are in-house fabricated MN (750 μm) and Adminpatch MN 1500 (1500 μm) and 1200 (750 μm) are chosen to investigate the effect of MN length on the penetration depth. Results show that the penetration depth of micro-particles increases from an increase of particle size, operating pressure and MN length.

In the following sections of this paper, the experimental results obtained from the previous work are compared with model results to verify the applicability of the model and further understand the MNs assisted micro-particles delivery.

**3.2.2.1. The effect of the operating pressure and particle size on penetration depth.** In general, operating pressure is one of the major variables which affect the momentum of the micro-particles and is expected to affect the penetration depths of the micro-particles inside a target. To confirm the significance of this effect, delivery of stainless steel micro-particles of 18 and 30 μm average diameters are simulated at operating pressure varies from 3 to 60 bar. The results of these simulations are presented in Fig. 10. In the figure, the solid lines represent the micro-particles delivery without the MN pierced holes and they correspond to the primary y axis (y1). The penetration depths of the micro-particles via the pierced hole are considered through the secondary y axis (y2). As can be seen, the results show that an increase of the operating pressure causes a slight increase in the penetration depth. It also shows that stainless steel micro-particles of 18 μm diameter can penetrate only from 0.58 to 2.59 μm in the skin (inside the stratum corneum) in the pressure ranging from 3 to 60 bar. However, a number of micro-particles delivered through the pierced holes penetrate into the dermis layer. The penetration depth inside the dermis layer is slightly more than the stratum corneum due to a decreased yield stress. As expected, the pierced hole has a greater effect on the penetration depth. The penetration depth rises from

1149.58 to 1151.66  $\mu\text{m}$  when Adminpatch MN 1500 is used for the pressure ranging from 3 to 60 bar. In addition, Fig. 10 shows the penetration depth of 18  $\mu\text{m}$  diameter of stainless steel micro-particles is less than 30  $\mu\text{m}$  diameter. The effect of the micro-particles size on the penetration depth is discussed in the following section.

The penetration depth of the micro-particles is also related to the size of the micro-particles which is one of the major variables that affects the particle momentum. As presented in Fig. 11, the diameter of the micro-particles shows a positive correlation with the penetration depth. In this figure, the results plotted in solid line are for the penetration of the micro-particles without pierced holes and are referred by the primary y axis. The secondary y axis explains the results plotted in the dashed line and show the maximum penetration depth of the micro-particles which goes through the pierced hole. The penetration depth is found to be

from 0.71 to 37.12  $\mu\text{m}$  in the top two layers of the skin (stratum corneum and viable epidermis layers) at operating pressure of 5 bar while the particle diameter ranges from 18 to 140  $\mu\text{m}$ . It indicates that the small micro-particles cannot penetrate further in the skin so much as they are rebounded by the skin due to the insufficient momentum. However, this condition may be fixed by the use of a MN array. As shown in Fig. 11, the penetration depth increases from 1149.75 to 1189.73  $\mu\text{m}$ , which is enhanced by delivering a number of micro-particles through the pierced holes created by the Adminpatch MN 1500. The penetration depth in dermis layer varies from 0.75 to 40.73  $\mu\text{m}$  which is more than the penetration in top layer.

A comparison between model and experimental results on penetration depths is shown in Fig. 12. Micro-particle penetration without (solid lines) and with (dashed lines) pierced holes refer to the primary and secondary axes, respectively. As can be seen, the

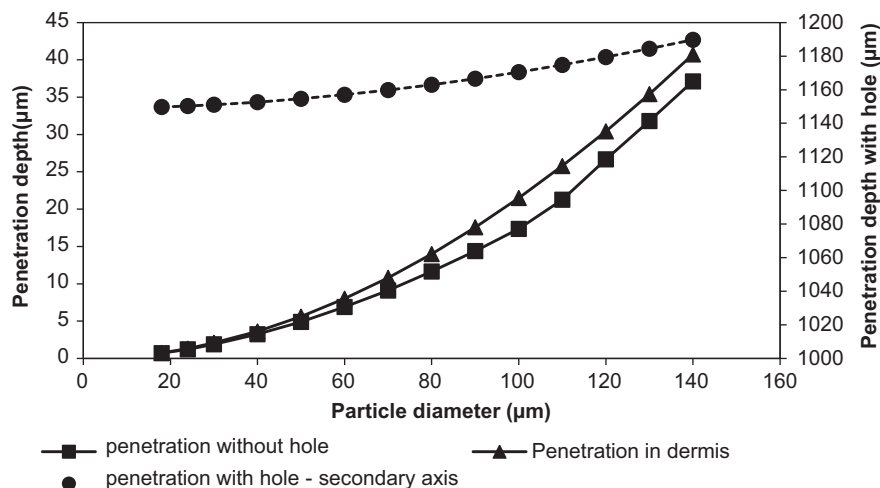


Fig. 11. The penetration depth of stainless steel micro-particles inside skin against the particle diameter (operating pressure: 5 bar; MN: Adminpatch MN 1500; solid line: primary y axis; dashed line: secondary y axis).

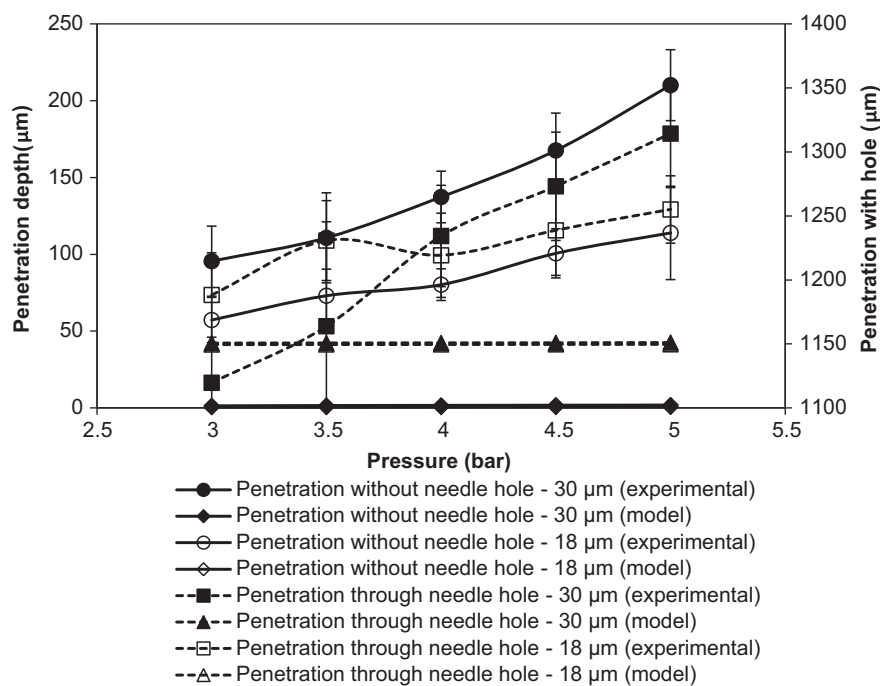


Fig. 12. A comparison between model and experimental results at various operating pressures (stainless steel micro-particles: 18 and 30 diameters; MN: Adminpatch MN 1500; solid line: primary y axis; dashed line: secondary y axis). The experimental results in the figure are generated from three repeats of experiments. Due to possible formation of agglomerates in the experiments, experimental and the modelling results do not match very well.



operating pressure and particle size have greater effects on the penetration depth for the experimental results. The penetration depth rises fast as the operating pressure is increased. It also shows a significant difference between stainless steel micro-particles of 18 and 30  $\mu\text{m}$  diameter, which demonstrates that an increased particle size has a positive correlation on the penetration depth. However, those two variables only have slight effects on the penetration depth according to the model result. This is because the pellet is considered to be separated into individual particles perfectly in the mathematical model which does not happen in practice. Zhang et al. (2013b) have used different pore sizes of meshes to break up the pellet separation and control the size distribution of the separated particles, which show that the pellet has been broken into individual particles effectively with only a few small agglomerated particles. These agglomerated particles may cause an increased penetration depth and further improve the effect of the operating pressure on the penetration.

Fig. 12 also shows that the micro-particles penetration through the pierced holes varies between model and experimental results. For the model result, the length of the pierced holes is considered to be a constant. Thus, the penetration difference between stainless steel micro-particles of 18 and 30  $\mu\text{m}$  diameters is only slight since the momentum of those two particles are insufficient to penetrate further in the skin. These differ with experimental results which show that the penetration depth varies at the operating pressure ranges from 3 to 5 bar. This is because the length of the pierced holes is varied after the removal of the MNs in the experiment. It directly affects the micro-particles penetration depth, such as small particles may penetrate further than larger particles. As presented in Fig. 12, the penetration depth of stainless steel micro-particles of 18  $\mu\text{m}$  diameter is more than 30  $\mu\text{m}$  diameter at 3 and 3.5 bar pressure. However, the experimental results show that the stainless steel micro-particles of 30 and 18  $\mu\text{m}$  diameters reach the penetration depth from 1119.7 to 1314.4  $\mu\text{m}$  and from 1188.3 to 1255.1  $\mu\text{m}$  while the pressure varies from 3 to 5 bar, respectively. The operating pressure only presents a slight effect at this condition. As expected, the length of the pierced holes becomes the primary factor which maximizes the penetration depth. It directly relates to the length of MN. The effect of the micro-needle length on the penetration depth is discussed in the following section.

**3.2.2.2. The effect of the micro-needle length.** In principle, the length of the pierced hole depends on the length of the micro-needle. An increased length of MNs causes an increase in the pierced holes and thereby increases the penetration depth of micro-particles. As presented in Fig. 13, the penetration depths of the micro-particles differ significantly between each application of MNs. Both model and experimental results present that the penetration depth increases from an increase of MN length. For the model result, the operating pressure does not show a great effect on the penetration depth. For the experimental result, the penetration depth is varied at the operating pressure ranges from 3 to 5 bar. This is because the effect of the agglomerates and the unmaintainable length of pierced holes, which are presented in previous section. The operating pressure presents a positive effect on the penetration depth, which agrees with the model result.

In conclusion, the experimental results match well with the model results in Fig. 13. It confirms that this mathematical model is suitable for modelling MNs assisted micro-particles delivery. It also indicates that the micro-particles can be deposited at a desired depth in a target based on a use of specific lengths of MNs. In addition, the penetration depth gradually increases with the increase in operating pressure. It can be considered that based on the assistance of the holes on the micro-particles delivery, the penetration depth can be fine tuned by the operating pressure.

### 3.3. Further discussions

In this paper, the penetration depths of micro-particles are analyzed with respect to variations in operating pressure, particle size, MN size using modelling and experimental results. It is evident that the particle penetration depth increases from an increase of the operating pressure and particle size as the particle momentum is related to those two key variables. In the experiments, the agglomerates provide a greater effect on the particle penetration depth. This is possibly why the model results could not match well with the experimental results in this paper. However, the agglomerates can be prevented by using a smaller pore size of mesh to allow individual micro-particles to pass through which provide obtain a uniform penetration depths of the particles and comparable well with model results.

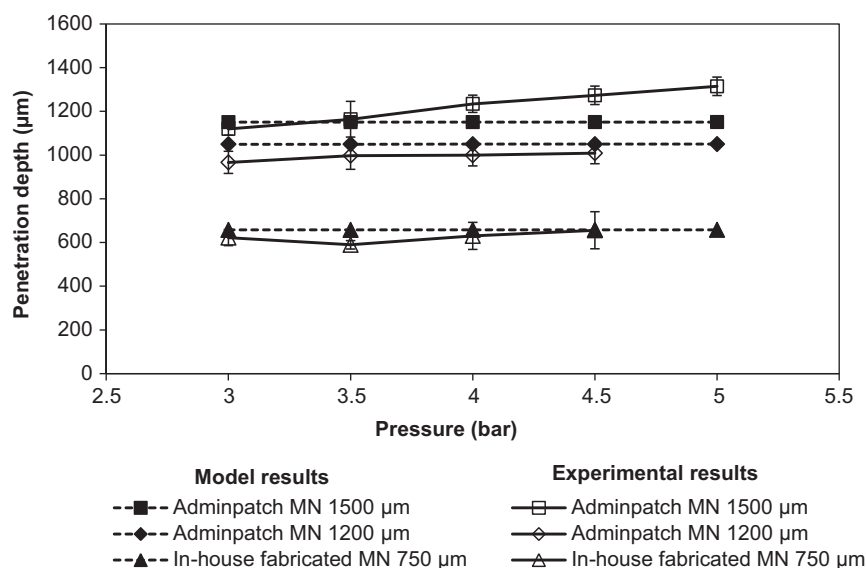


Fig. 13. The effect of the micro-needle length on the penetration depth of the stainless steel micro-particles (30  $\mu\text{m}$ ). The experimental results in the figure are generated from three repeats of experiments.

The paper confirms that an application of MN array provides a positive effect on the micro-particles penetration. The maximum penetration depth of the micro-particles has presented a significant increment from the results without MN application. For the MN assisted micro-particles delivery, the penetration depth reaches the dermis layer inside skin, which was not achieved in the previous gene gun systems (e.g., injection jet, light gas gun, contoured shock tube, etc). Mitchell et al. (2003) have used a light gas to accelerate the stainless steel micro-particles of 25  $\mu\text{m}$  diameter to a velocity of 170 m/s (20 bar) and penetrate 150  $\mu\text{m}$  into excised canine buccal mucosa. Kendall et al. (2001) have suggested that the  $1 \pm 0.2$   $\mu\text{m}$  diameter gold particles can reach a velocity of  $580 \pm 50$  m/s at 40 bar pressure using a contoured shock tube and penetrate 66  $\mu\text{m}$  in the skin. The epidermis has been normally considered as the target tissue for gene loaded particle delivery as the devices may be limited by the penetration depth they achieve (Trainer and Alexander, 1997). Now the target tissue may be the dermis layer as the use of MNs promise to increase the penetration depths further. In other words, the MN may be useful for the injection of micro-particles especially for the targets which require a deeper injection of the particles.

#### 4. Conclusions

A mathematical model has been developed for MN assisted micro-particles delivery from gene guns. MN assisted micro-particles delivery, and in particular the penetration depths of the particles, are studied in this paper. For the acceleration stage, the particle velocity is analysed in relation to the operating pressure and these results compare well with the experimental results obtained from the previous work (Zhang et al., 2013b). For the deceleration stage, an individual micro-particle trajectory has been simulated in the model. Additionally, the distribution of the micro-particles in three different layers has been determined using modelling results. These results show that about 75% of particles penetrate into the stratum corneum without going through the holes, and 23 and 2% of particles penetrate into epidermis and dermis layers via the pierced holes, respectively. The presented model for MN assisted micro-particles delivery takes into consideration possible change in operating pressure, particle size, MN length due to the micro-particles delivery is directly related to those key variables. Model results obtained indicate that increasing the operating pressure and particle size would increase the penetration depth of the micro-particles inside skin due to the increased momentum. In addition, the hole length is shown to be a major variable which maximizes the particle penetration depth. The model results match well with the experimental results for the penetration depth of micro-particles. In conclusion, the presented model is shown to be useful for simulating micro-particle trajectories and penetration depth for MN assisted micro-particles delivery.

#### Conflicts of interest

The authors declare no conflict of interest.

#### Acknowledgements

Loughborough University (UK) is acknowledged for providing a PhD studentship to Dr Dongwei Zhang which made this work possible. Furthermore, the technical supports from Mr. Tony Eyre, Mr. Mark Barron, Mr. Jim Muddimer, Mr. Terry Neale and Mr. Steve Bowler are gratefully acknowledged.

#### Appendix A

The drag coefficient as function of particle Reynolds number, as used in this work (Morsi and Alexander, 1972)

$$\begin{aligned} C_d &= 24.0/\text{Re} && \text{for } \text{Re} < 0.1, \\ C_d &= 22.73/\text{Re} + 0.0903/\text{Re}^2 + 3.69 && \text{for } 0.1 < \text{Re} < 1.0, \\ C_d &= 29.1667/\text{Re} - 3.8889/\text{Re}^2 + 1.222 && \text{for } 1.0 < \text{Re} < 10.0 \\ C_d &= 46.5/\text{Re} - 116.67/\text{Re}^2 + 0.6167 && \text{for } 10.0 < \text{Re} < 100.0 \\ C_d &= 98.33/\text{Re} - 2778/\text{Re}^2 + 0.3644 && \text{for } 100.0 < \text{Re} < 1000.0 \\ C_d &= 148.62/\text{Re} - 4.75 \times 10^4/\text{Re}^2 + 0.357 && \text{for } 1000.0 < \text{Re} < 5000.0 \end{aligned}$$

#### References

- Al-Qallaf, B., Das, D.B., Davidson, A., 2009. Transdermal drug delivery by coated microneedles: geometry effects on drug concentration in blood. *Asia-Pac. J. Chem. Eng.* 4 (6), 845–857, <http://dx.doi.org/10.1002/apj.353>.
- Bellhouse, B.J., Sarphie, D.F., Greenford, J.C., 1994. Needleless Syringe Using Supersonic Gas Flow for Particle Delivery. International Patent WO94/24263.
- Bellhouse, B.J., Bell, J., Millward, H.R., Phillips, M.J., Nabulsi, S.M., 2003. Particle Delivery, US Patent US 6592545 B1.
- Bellhouse, B.J., Greenford, J.C., Sarphie, D.F., 2006. Particle Delivery, European Patent EP 1637173 A2.
- Chen, D., Maa, Y.F., Haynes, J.R., 2002. Needle-free epidermal powder immunization. *Expert Rev. Vaccines* 1 (3), 265–276.
- Cheung, K., Han, T., Das, D.B., 2014. Effect of force of microneedle insertion on the permeability of insulin in skin. *J. Diabetes Sci. Technol.* 8 (3), 444–452, <http://dx.doi.org/10.1177/1932296813519720>.
- Crozier, W.D., Hume, W., 1957. High velocity light gas gun. *J. Appl. Phys.* 28 (8), 892–895.
- Dehn, J., 1987. A unified theory of penetration. *Int. J. Impact Eng.* 5, 239–248.
- Donnelly, R.F., Garland, M.J., Singh, T.R.R., Migalska, K., Majithiya, R., McCrudden, C. M., Kole, P.L., Mahmood, T.M.T., McCarthy, H.O., Willson, A.D., 2012. Hydrogel-forming microneedle array for enhanced transdermal drug delivery. *Adv. Funct. Mater.* 22, 4879–4890.
- Duck, F.A., 1990. *Physical Properties of Tissue: A Comprehensive Reference Book*. Academic Press, Harcourt Brace Jovanovich, London.
- Eberly, D., 2002. Rotation Representations and Performance Issue, Geometric Tools, LLC (<http://www.geometrictools.com/Documentation/RotationIssues.pdf>) [Accessed on 3/6/2013].
- Han, T., Das, D.B., 2013. Permeability enhancement for transdermal delivery of large molecule using low-frequency sonophoresis combined with microneedles. *Journal of Pharmaceutical Sciences* 102 (10), 3614–3622.
- Holbrook, K.A., Odland, G.F., 1974. Regional Differences in the thickness (cell layers) of the human stratum corneum: an ultrasound analysis. *J. Invest. Dermatol.* 62, 415–422.
- ImageJ, 2013. ImageJ (<http://rsbweb.nih.gov/ij/disclaimer.html>) [Accessed on 3/6/2013].
- Kendall, M.A.F., Carter, F.V., Mitchell, T.J., Bellhouse, B.J., 2001. Comparison of the transdermal ballistic delivery of micro-particle into human and porcine skin. In: *Proceedings of the 23rd Annual International Conference of the IEEE*, 2991–2994.
- Kendall, M.A.F., Quinlan, N.J., Thorpe, S.J., Bellhouse, B.J., Ainsworth, R.W., 2004a. Measurements of the gas and particle flow within a converging-diverging nozzle for high speed powdered vaccine and drug delivery. *Exp. Fluids* 37, 128–136.
- Kendall, M.A.F., Rishworth, S., Carter, F., Mitchell, T., 2004b. Effects of relative humidity and ambient temperature on the ballistic delivery of micro-particles to excised porcine skin. *J. Invest. Dermatol.* 122, 739–746.
- Kishino, A., Yanagida, T., 1988. Force measurements by micromanipulation of a single actin filament by glass needles. *Nature* 334, 74–76.
- Lambert, P.H., Laurent, P.E., 2008. Intradermal vaccine delivery: will new delivery systems transform vaccine administration? *Vaccine* 26, 3197–3208.
- Lin, M., 2000. The gene gun: current applications in cutaneous gene therapy. *Int. J. Dermatol.* 39, 161–170.
- Liu, Y., 2006. Physical-mathematical modeling of fluid and particle transportation for DNA vaccination. *Int. J. Eng. Sci.* 44 (15–16), 1037–1049.
- Liu, Y., 2007. Impact studies of high-speed micro-particle following ballistic delivery. *IEEE Trans. Biomed. Eng.* 54 (8), 1507–1513.
- Matteucci, M., Fanetti, M., Casella, M., Gramatica, F., Gavioli, L., Tormen, M., Greci, G., De Angelis, F., Di Fabrizio, E., 2009. Poly vinyl alcohol re-usable masters for MN replication. *Microelectron. Eng.*, <http://dx.doi.org/10.1016/j.mee.2009.01.068>.
- McAllister, D.V., Wang, P.M., Davis, S.P., Park, J.H., Canatella, P.J., Allen, M.G., Prausnitz, M.R., 2003. Microfabricated needles for transdermal delivery of macromolecules and nanoparticles: fabrication methods and transport studies. *Proc. Nat. Acad. Sci. U.S.A.* 100, 13755–13760.
- Mitchell, T.J., Kendall, M.A.F., Bellhouse, B.J., 2003. A ballistic study of micro-particle penetration to the oral mucosa. *Int. J. Impact Eng.* 28, 581–599.

- Morsi, S.A., Alexander, A.J., 1972. An investigation of particle trajectories in two-phase flow systems. *J. Fluid Mech.* 55 (2), 193–208.
- Nayak, A., Das, D.B., 2013. Potential of biodegradable microneedles as a transdermal delivery vehicle for lidocaine. *Biotechnol. Lett.* 35 (9), 1351–1363.
- Nayak, A., Das, D.B., Vladislavljević, G.T., 2014. Microneedle-assisted permeation of lidocaine carboxymethylcellulose with gelatine co-polymer hydrogel. *Pharm. Res.* 31 (5), 1170–1184.
- O'Brien, J.A., Lummis, S.C.R., 2006. Biolistic transfection of neuronal cultures using a hand-held gene gun. *Nature Protocols* 1 (2), 977–981.
- Parker, F., 1991. Structure and Function of the Skin: Paper 1 in *Dermatology*. In: Orkin, M., Maibach, H.I., Dahl, M.V. (Eds.), first ed. Appleton and Lange, Norwalk, Connecticut.
- Phipps, J.B., Padmanabhan, R.V., Lattin, G.A., 1988. Transport of ionic species through skin. *Solid State Ionics* 28, 1778–1783.
- Olatunji, O., Das, D.B., 2010. Painless drug delivery using microneedles. *Current Technologies to Increase the Transdermal Delivery of Drugs* ((Eds.), Joan Escobar Chavez). Bentham Science Publishers (available online at ([http://www.benthamdirect.org/pages/b\\_getarticlebybook.php](http://www.benthamdirect.org/pages/b_getarticlebybook.php))). 978-1-60805-191-5.
- Olatunji, O., Das, D.B., 2011. Drug delivery using microneedles. In: Zhanfeng, C.u.i. (Ed.), *Comprehensive Biotechnology*, second ed. Elsevier, The Boulevard, Langford Lane, Oxford, United Kingdom (MS number 501. MRW, ISBN:13:978-0-444-53352-4).
- Olatunji, O., Das, D.B., Nassehi, V., 2012. Modelling transdermal drug delivery using microneedles: effect of geometry on drug transport behaviour. *Journal of Pharmaceutical Sciences* 101 (1), 164–175.
- Olatunji, O., Das, D.B., Garland, M.J., Belaid, L., Donnelly, R.F., 2013. Influence of Array interspacing on the force required for successful microneedle skin penetration: theoretical and practical approaches. *Journal of Pharmaceutical Sciences* 102 (4), 1209–1221.
- Olatunji, O., Igwe, C.C., Ahmed, A.S., Alhassan, O.A., Asieba, G.O., Das, D.B., 2014. Microneedles from fish scale biopolymer. *J. Appl. Polym. Sci.* 131 (12), <http://dx.doi.org/10.1002/app.40377>.
- Quinlan, N.J., Kendall, M.A.F., Bellhouse, B.J., Ainsworth, R.W., 2001. Investigations of gas and particle dynamics in first generation needle-free drug delivery device. *Shock Waves* 10, 395–404.
- Rushmer, R.F., Buettner, K.J.K., Short, J.M., Odland, G.F., 1966. The skin. *Science* 154, 343–348.
- Schaefer, H., Redelmeier, T.E., 1996. *Skin Barrier: Principles of Percutaneous Absorption*. Karger, New York.
- Scheuplein, R.J., Blank, I.H., 1971. Permeability of the skin. *Physiol. Rev.* 51, 702–747.
- Shampine, L.F., Reichelt, M.W., 1997. The matlab ode suite. *SIAM J. Sci. Comput.* 18 (1), 1–22.
- Soliman, S.M., Abdallah, S., Gutmark, E., Turner, M.G., 2011. Numerical simulation of microparticles penetration and gas dynamics in an axisymmetric supersonic nozzle for genetic vaccination. *Powder Technol.* 208, 676–783.
- Trainer, A.T., Alexander, M.Y., 1997. Gene delivery to the epidermis. *Hum. Mol. Gen.* 6 (10), 1761–1767.
- Truong, N.K., Liu, Y., Kendall, M.A.F., 2006. Gas and particle dynamics of a contoured shock tube for pre-clinical micro-particle drug delivery. *Shock Waves* 15, 149–164.
- Webster, C., 1995. The discovery of Boyle's law, and the concept of the elasticity of air in the seventeenth century. *Arch. Hist. Exact Sci.* 2, 441–502.
- Wildnauer, R.H., Bothwell, J.W., Douglas, A.B., 1971. Stratum corneum properties I. Influence of relative humidity on normal and extracted stratum corneum. *J. Invest. Dermatol.* 56, 72–78.
- Yager, E.J., Stagnar, C., Gopalakrishnan, R., Fuller, J.T., Fuller, D.H., 2013. Optimizing particle-mediated epidermal delivery of an influenza DNA vaccine in ferrets. *Methods Mol. Biol.* 940, 223–237.
- Yang, C.H., Shen, S.C., Lee, J.C., Wu, P.C., Hsueh, S.F., Lu, C.Y., Meng, C.T., Hong, H.S., Yang, L.C., 2004. Seeing the gene therapy: application of gene gun technique to transfect and decolour pigmented rat skin with human agouti signalling protein cDNA. *Gene Ther.* 11 (13), 1033–1039.
- Zhang, M.J., Tao, W.M., Pianetta, P.A., 2007. Dynamics modeling of biolistic gene guns. *Phys. Med. Biol.* 52, 1485–1493.
- Zhang, D.W., Das, D.B., Rielly, C.D., 2013a. Potential of microneedle assisted micro-particle delivery by gene guns: a review. *Drug Delivery*, <http://dx.doi.org/10.3109/10717544.2013.864345> (in press).
- Zhang, D.W., Das, D.B., Rielly, C.D., 2013b. An experimental study of microneedles assisted micro-particle delivery using a model system. *Journal of Pharmaceutical Sciences* 102 (10), 3632–3644.
- Zhang, D.W., Das, D.B., Rielly, C.D., 2014a. Microneedles assisted micro-particles delivery from gene guns: experiments using skin mimicking agarose gel. *Journal of Pharmaceutical Sciences* 103 (2), 613–627.
- Zhang, D.W., Das, D.B., Rielly, C.D., et al., 2014b. Microneedle Assisted Micro-particle Delivery by Gene Guns: Experiments and Modelling on the Effects of Particle Characteristics. *Drug Delivery*, <http://dx.doi.org/10.3109/10717544.2014.887158> (in press).